Article

Isotopic Enrichment Resulting from Differential Condensation of Methane Isotopologues Involving Non-equilibrium Gas−Surface Collisions Modeled with Molecular Dynamics Simulations

Michelle R. Brann, Xinyou Ma, and S. J. Sibener*

Read Online

ACCESS | 📊 Metrics & More | 📰 Article Recommendations

ABSTRACT: We employ molecular dynamics simulations to understand the energy transfer processes involved during the collisions of CH_4 and CD_4 with CH_4 layered surfaces at 20 K in order to explain our experimental finding of preferential adsorption of CD_4 compared to CH_4. There is good agreement between our MD simulations and our experimental results. We find that gas−surface collisional energy accommodation is dominated by exchange involving the translational degrees of freedom of the incident molecule and intermolecular vibrations of the interface. This observation allows us to understand that the cause of CD_4

preferential sticking arises from its propensity to lose more energy during its first impact with the surface, inducing longer residence times and leading to increased probability of becoming trapped and condensed onto the surface. Systematic trends are seen for sticking probabilities and energy transfer when we explore the behavior of the other H/D-substituted isotopologues of methane. These molecular insights provide context into the adsorption behavior occurring on icy dust grains in our solar system. Because adsorption is often the first step, trapping efficiency differences between isotopologues have notable implications for condensed phase reaction probabilities involving isotopically substituted species and subsequent events leading to increased molecular complexity. Aside from astrophysical significance, our findings have direct implications for novel isotope enrichment mechanisms under non-equilibrium conditions involving the preferential condensation of heavier isotopes and isotopologues during gas−surface collisions under specifically selected substrate, gas mixture, and incident kinematic conditions.
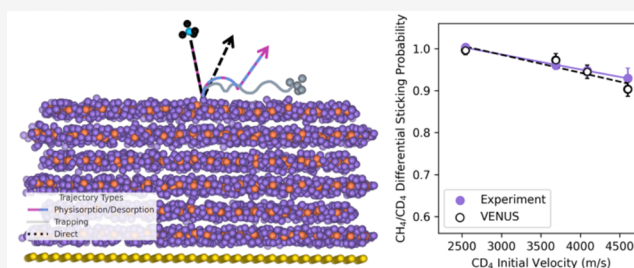
INTRODUCTION

Understanding energy-transfer dynamics at the gas−surface interface helps to accurately model a variety of chemical and physical phenomena.[1,2] The energy transfer that occurs when a gas molecule collides with a condensed surface is complicated and a result of many factors such as the gas−surface potential, translational energy and incident kinematics of the projectile, gas−surface mass ratio, density of states of the interface's degrees of freedom, surface morphology, and surface temperature. We present detailed molecular dynamics simulations to explicitly calculate energy transfer with the surface in order to understand our experimental observation[3] that preferential adsorption occurs for CD_4 when striking the CH_4 surface compared to CH_4 under non-equilibrium gas−surface collision conditions.

In general, adsorption is a key process in both astrophysical and terrestrial environments because it is the first step in many gas−surface interactions.[4−6] In extraterrestrial environments where chemical species are scarce, adsorption onto an interstellar grain, planetesimal, or other larger body dictates whether more complex organic molecules can form.[7−12] In order to accurately model chemical abundances, we previously

examined isotopologues to understand how differences in mass between the projectile and the surface influence the ability of the species to adsorb and thus lead to observed relative isotopic abundances.[13,14] We studied methane and its isotopologue deuterated methane due to methane's interstellar abundance in both the gaseous and solid forms[15−21] and its ability to form larger hydrocarbon species through addition reactions.[22] We determined, through two independent experimental methods (monitoring reflected species as well as those species adsorbed on the surface), that preferential sticking and condensation occurred for CD_4 compared CH_4 under specific non-equilibrium gas−surface collision conditions.[3]

Molecular dynamics simulations of gas−surface collisions provide fundamental details of reaction dynamics, energy
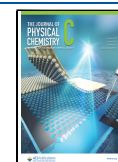
transfer, and product states for gas−surface reactions at the atomistic level, where the gas−surface interaction is described by a multidimensional potential energy surface.[1,23−31] For isotopologues, the gas−surface potentials are intrinsically identical; hence, any difference in sticking probabilities is directly correlated to the dynamics of the gas−surface collision. Here, we refine our computational parameters and perform molecular dynamics (MD) simulations using VENUS[23] to fully investigate this energy transfer during the collision of CH_4 and CD_4 with CH_4 layered surfaces that results in these differing trapping efficiencies. We conclude that the dominant energy exchange occurs between the incident translational degrees of freedom and intermolecular lattice surface vibrations. Because CD_4 loses more translational energy upon impact compared to CH_4, the CD_4 projectiles interact with the surface longer and are therefore more likely to be trapped onto the surface.

Understanding the refined details of intermolecular energy exchange responsible for gaseous condensation is in itself quite important as it has a direct linkage to many technological applications. One such avenue pertains to water condensation in high-velocity gas flows as experienced by aircraft in low-temperature situations, while another example is condensation on windmill blades for power generation operating in cold environments.

Additionally, these findings can be incorporated into the development of novel heterogeneous isotopic enrichment and separation techniques. More broadly, this work is also critical to understanding the nature of methane adsorption within astrophysical environments. Trapping efficiency differences and energy exchange mechanisms can be incorporated into astrophysical models to explain molecular abundances and increased deuterium abundance in cometary ices and outer solar system planets. Moreover, aside from astrophysical environments, adsorption has implications into fields such as heterogeneous catalysis or thin film growth where the adsorption process serves as the first step in film formation.[32]

COMPUTATIONAL DETAILS

Potential Energy Surface. As detailed in our earlier publication and summarized here,[3] the potential energy function for the $(CH_4)_{beam}$ and $(CH_4)_{surface}$ on top of a Au(111) crystal is given by

$$V = V_{beam} + V_{surface} + V_{beam+surface} \qquad (1)$$

where V_{beam} is the beam CH_4 intramolecular potential, $V_{surface}$ is composed of intramolecular CH_4 potentials (same as V_{beam}) as well as the intermolecular CH_4−CH_4 and Au−CH_4 potentials using the 6−12 Lennard-Jones formulation, and $V_{beam+surface}$ is the intermolecular CH_4−CH_4 potential. Each intramolecular CH_4 potential is expressed as a sum of Morse potentials for the C−H stretches and quadratic potentials for the H−C−H bends: the Morse parameters are $D = 4.878$ eV, $\beta = 1.86$ Å^{-1}, and $r_0 = 1.086$ Å,[28] and each HCH quadratic bend has $f = 0.585$ mdyn Å/rad^2 and $\theta = 109.47°$.[28,33] These parameters were also used for the CD_4 beam. The methane harmonic frequencies are 3193, 3021, 1583, and 1413 cm^{-1}.

The surface model consists of 6 methane layers stacked in an AB sequence on top of a layer of gold to form a cubic close-packed structure (Figure 1).[34] There are 789 CH_4 molecules in alternating layers of 120/143 molecules to prepare a methane surface area of 1600 Å^2 (40 × 40 Å^2 in the x−y plane). The total surface height of all of the stacked layers is 18 Å including the gold layer on the bottom. All intermolecular potentials are
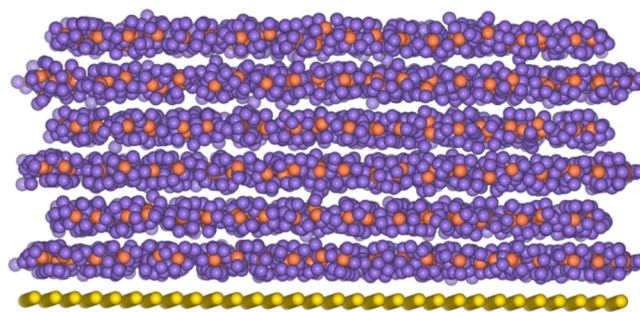
Figure 1. Schematic model of the optimized methane surface comprised of methane layers on top of a layer of gold. The methane surface area is 1600 Å^2 and is in a cubic close-packed structure.

written as sums of 6−12 Lennard-Jones two-body potentials with a cutoff distance of 10 Å and are summarized in Table 1.[35,36] For the Au(111) base, $\varepsilon_0 = 0.229$ eV and $\sigma_0 = 2.951$ Å[37]

Table 1. Parameters of the Lennard-Jones 12−6 Atom−Atom Interactions

|	ε_0 (eV)	σ_0 (Å)
Au−Au	0.2294	2.951
C−C	0.0044	3.35
C−H	0.0021	2.99
H−H	0.0004	2.61
Au−C	0.0318	2.99
Au−H	0.0	0.0

were used to give an atomic spacing of 2.93 Å, closely matching that determined from STM images of the reconstructed (111) surface.[38] In the current surface model, the CH_4 molecules are spaced by an average C−C distance of 3.8 Å, which is comparable to calculated CH_4 intermolecular potentials.[39] The Au−CH_4 interactions are described by Au−C Lennard-Jones potentials with parameters derived from the Au−Au and C−C interactions using standard mixing rules,[37,40] which are $\varepsilon_0 = 0.0318$ eV and $\sigma_0 = 2.99$ Å.

Prior to trajectory simulations, the surface configuration was fully relaxed to a potential energy minimum after a geometry optimization step and a thermal equilibration step at 20 K. The surface configuration at 20 K is similar to a flat crystalline surface, which is a model representation of a local section of the experimental methane surface prepared from beam deposition of methane on a Au(111) substrate, which in reality may contain domains of small, imperfect crystallites. However, even with this difference, there is qualitatively similar energy-transfer dynamics and thus appropriate to use for our study.[29]

Although the surface retains a layered crystalline configuration of methane molecules in the z-direction at 20 K, the orientations of the hydrogens of a particular methane molecule within a layer are randomized. Thus, as the surface relaxes into its configuration, there may be some regions that can adsorb incident projectiles more efficiently.

The easiest test to determine a small radial area acceptable for gas−surface collision simulations is to calculate the methane binding enthalpy with different impact parameters (BMAX, Å) where BMAX is the radial distance in angstroms in the X−Y plane from a head on collision to a methane on the surface. A microcanonical ensemble averaged intermolecular potential curve for CH_4 approaching the surface is obtained by

averaging the potential energies of over 1000 randomly oriented CH_4 molecules as a function of CH_4−surface distance.[41] Comparing the interfacial potential energy curves evaluated at several BMAX impact parameters (Figure 2), we
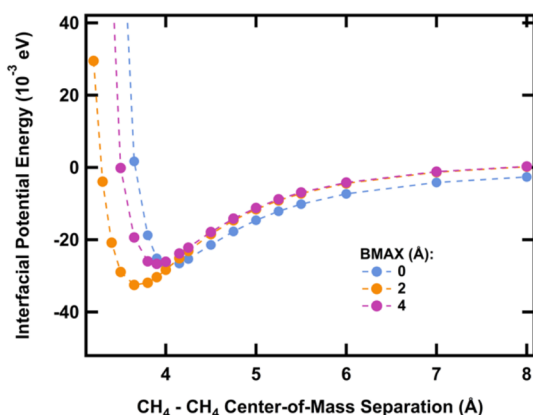
Figure 2. Orientation averaged CH_4 (beam)−CH_4 (surface) intermolecular potential. The incident methane experiences a slightly different potential based on where it hits on the unit cell.

find that the potential minimum decreases as the impact parameter traverses the unit cell. The potential energy curve at 4 Å is close to the curve at 0 Å, but not identical because our average C−C distance is 3.8 Å. We then decided to use a BMAX impact parameter of 8 Å to sample the equivalence of two unit cells for a representative sampling of the surface.

Procedure for the Molecular Dynamics Simulations. Molecular dynamics simulations were performed using the VENUS general chemical dynamics computer program.[23,42] Classical trajectories were used to simulate collisions of a beam of CH_4 or CD_4 with the CH_4 surface. Initial conditions for the trajectories were selected to sample the beam's translational and vibrational energy at the experimental conditions; rotations were frozen at 0 K given the supersonic expansion of the incident beam. The selection of initial conditions follows from previous VENUS studies.[30,43] For each simulation, a

beam of colliding molecules was aimed at a circular area. Each trajectory was initialized with a separation of 10 Å between the center-of-mass of the beam molecule and the surface aiming point. Unless otherwise specified (in the simulations with an angle of 45° between the beam and the surface), the beam molecule collides perpendicularly to the surface to match the predominant configuration of the experimental apparatus. For each beam, the initial vibrational levels were sampled from Boltzmann distributions at 300, 700, 900, or 1100 K including the vibrational zero-point energy. Our experimental studies employ essentially monoenergetic seeded supersonic beams so that the CH_4 and CD_4 have the same incident velocity but different kinetic energies and momenta (0.49, 1.16, 1.48, and 1.79 eV for CH_4 and 0.67, 1.41, 1.74, and 2.19 eV for CD_4).

We also ran classical trajectories to simulate collisions of a beam of CH_3D, CH_2D_2, and CD_3H with the CH_4 surface. These trajectories were compared to those of the 1.79 eV CH_4 and 2.19 eV CD_4 beams (the highest initial velocity, 4613 m/s). Thus, the initial vibrational levels were sampled from a Boltzmann distribution at 1100 K, and the rotational levels were frozen at 0 K. The kinetic energies were 1.93 2.02, and 2.1 eV for CH_3D, CH_2D_2, and CD_3H, respectively.

For each trajectory, the gold and bottom three layers were held rigid and acted as anchor layers. Additionally, the mass of carbon atoms in rim CH_4 molecules was artificially increased by 10000 to truncate the surface. Initial conditions for this surface were selected by assigning velocities to the carbon atoms of these layers, sampled from a Maxwell−Boltzmann distribution at 20 K. The surface was equilibrated by a 50 ps molecular dynamics simulation with velocity scaling every 1000 steps and another equilibration without velocity scaling. The trajectories were propagated with a Velocity-Verlet integrator with a time step of 0.01 fs. Trajectories were terminated either when the distance between the central methane molecule and the outgoing product exceeded 30 Å or when the total integration exceeded 50 ps. Typically, 1900−2000 trajectories were calculated for each ensemble of initial conditions, including the surface composition and beam conditions.
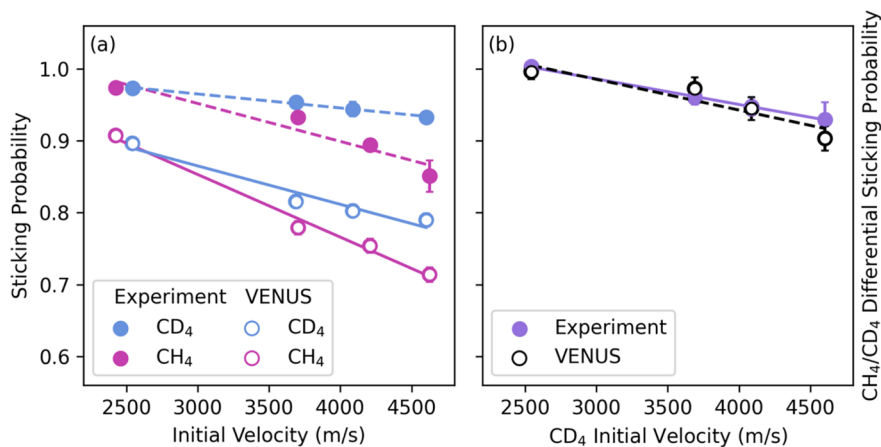
Figure 3. Sticking probabilities (a) calculated from the number of CH_4 and CD_4 direct and physisorption scattering trajectories (open circles) on a CH_4 surface at 20 K. Error bars represent the standard error of a binomial distribution of at least 1900 trajectories for each velocity. The experimental sticking probabilities (solid circles)[3] are from at least three King and Wells measurements on at least three different days. The differential sticking probability (b) is the ratio of the CH_4/CD_4 sticking probability at the CD_4 initial velocity. The experimental and VENUS CH_4 sticking probabilities are extrapolated using the linear fit in (a), so that the ratio is taken at the same initial condition. Excellent agreement between experiment and theory is readily seen in (b).
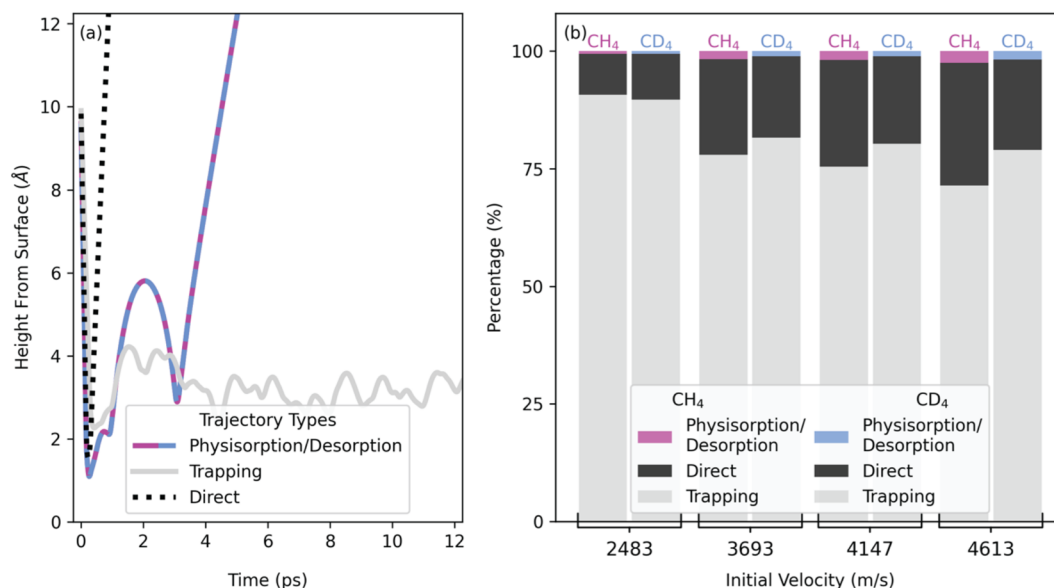
Figure 4. (a) Example representative trajectory types plotted as center-of-mass height from the surface versus time. Direct scattering trajectories have one ITP, physisorption/desorption trajectories have MITPs, and trapped trajectories have MITPs and remain on the surface after 50 ps. (b) Percentage (%) of each trajectory type for the CH_4 and CD_4 projectiles at each incident velocity. A total of 1922 to 1979 MD trajectories were run for each incident condition.

■ RESULTS AND DISCUSSION

Sticking Probability. First, the theoretical predictions of the sticking probabilities from the trajectory simulations agree well with the experimentally determined sticking probabilities. Computationally, the sticking probability is the fraction of trajectories with CH_4 or CD_4 remaining on the surface after 50 ps. Our VENUS calculations demonstrate (1) a decrease in sticking probability with increasing incident velocity as well as (2) a significant isotopic effect as seen in the difference between CH_4 and CD_4 sticking probabilities on the CH_4 surface (Figure 3) as a function of incident velocity. *In general, we find that the CD_4 and CH_4 sticking probabilities are identical for the lowest velocity beam before diverging for the higher velocity beams as more CD_4 trajectories become preferentially trapped on the surface.* For comparison, the VENUS calculations are overlaid with our experimental King and Wells[44] sticking probability measurements (solid circles).[3] Although the theoretical sticking probabilities are slightly lower than the experimental values, the trend and differential sticking between CH_4 and CD_4 at each initial condition are in excellent agreement (Figure 3b). This offset could result from structural differences between our disordered experimental surface and our layered flat theoretical surface. Additionally, Lennard-Jones potentials are not fully optimized for the repulsive region.[45] Regardless, there is qualitatively similar energy-transfer dynamics between crystalline and domains of small, imperfect crystallites[29] so that we can use our theoretical system to explain how the two isotopologues are differentially condensed.

Direct/Indirect Scattering. The trajectories that eventually scattered off the surface can experience different dynamics on the surface. In particular, these trajectories are categorized as two types: (1) direct scattering with only 1 inner turning point (ITP) and (2) physisorption/desorption with multiple ITPs, where an ITP occurs when the CH_4/CD_4 center-of-mass height changes from decreasing to increasing.[30] Representative CH_4 trajectories of both types at an incident

velocity of 4613 m/s are shown in Figure 4a as well as a comparison to a sticking/trapped trajectory, where the center-of-mass height from the layered surface is plotted as a function of time. The direct scattering trajectory bounces on the surface with a shorter residence time near the surface, while the physisorption/desorption trajectory can experience multiple hops on the surface until a successful escape from the surface. The trapped trajectory remains about 3.5 Å above the surface, in agreement with the CH_4-CH_4 intermolecular Lennard-Jones potentials and surface spacing. At our selected incident velocities, we do not find any CH_4 or CD_4 projectiles contain enough incident energy to penetrate into the bulk film.

Separating the scattered trajectories into direct and physisorption/desorption trajectories, we find that with increasing incident velocity, the percentage of direct trajectories and physisorption/desorption trajectories both increase as fewer projectiles are trapped on the surface. Additionally, the relative percentage of direct trajectories compared to physisorption/desorption trajectories decreases. This difference is particularly stark for the highest velocity (4613 m/s) beam where among the scattered trajectories there is a larger percentage of direct trajectories for CH_4 than for CD_4. This provides mechanistic support for why trapping efficiencies differ between these two isotopologues and how energy loss to the surface plays an important role.

Scattered Trajectory Energy Distributions. For each trajectory that does not stick on the surface, we conducted additional analyses to determine the post-collision velocity distributions, translational and internal energy lost to the surface, residence time on the surface, and angle scattered from the surface. When CH_4 and CD_4 collide with the CH_4 surface, in order for trapping to occur, the CH_4 or CD_4 molecule must lose enough of its initial energy to avoid bouncing back. To align with our experimental setup employing monoenergetic seeded supersonic beams, the molecular dynamics simulations consider CH_4 and CD_4 molecules with identical incident velocities but different kinetic energies and momenta. Thus, we
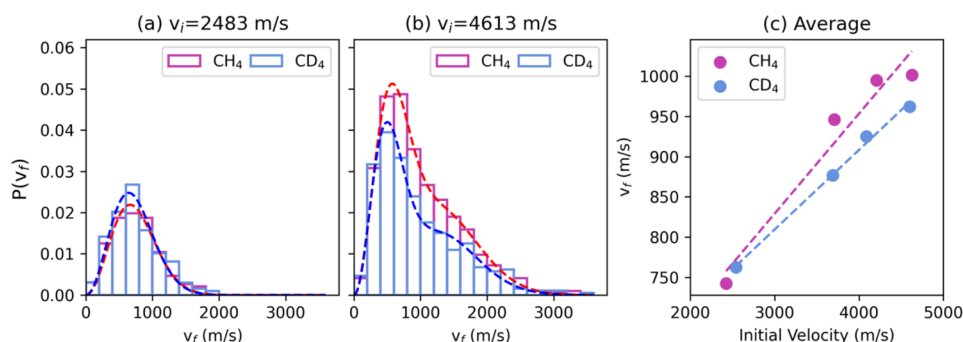
Figure 5. Final velocity distributions for CH_4 and CD_4 scattering off of a CH_4 surface at 20 K. The velocity is calculated from the momenta at the final step of the trajectory. The distributions are curve fit to either one Maxwell−Boltzmann distribution (panel a, v_i = 2483 m/s) or the sum of two Maxwell−Boltzmann distributions (panel b, v_i = 4613 m/s). The average final velocity is plotted in (c). As the incident velocity increases, the projectiles scatter off with an average faster final velocity; CH_4 scatters off with a higher velocity.
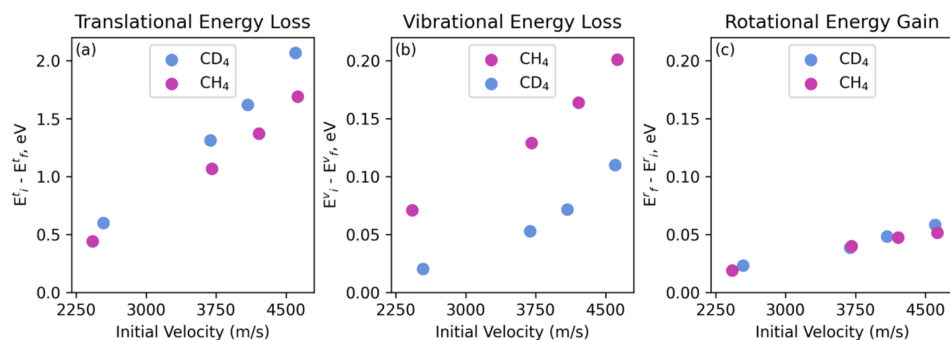
Figure 6. Average translational energy loss (a), vibrational energy loss (b), and rotational energy gain (c) for CH_4 and CD_4 scattering off a CH_4 surface at 20 K. The translational energy (a) is calculated from the momenta at the final step of the trajectory. The vibrational energy (b) is calculated from the momenta at the final step of the trajectory and using the harmonic bend and Morse parameters for methane. The rotational energy (c) is calculated from the angular momentum evaluated at the final step of the trajectory. Energy loss is calculated by taking the initial − final energy (in eV) for each scattered trajectory. Because the initial rotational energy is 0, the rotational energy gained (final − initial) is equal to the final energy (in eV). Translational energy exchange is an order of magnitude higher than vibrational and rotational energy exchange with the surface and is responsible for trapping the methane molecules.

first examine the final velocity distributions for the projectiles that scatter off the surface (Figure 5a,b) before calculating the translational energy exchange to the surface.

As expected, with increasing incident velocity, the scattered molecules leave the surface with a higher final velocity. For the lowest incident velocity (2483 m/s) molecules, there is essentially no difference between CH_4 and CD_4. However, when the incident velocity is increased to 4613 m/s, the CH_4 molecules scatter with a larger final velocity (Figure 5b). The velocity distributions are well described by either one or the sum of two Maxwell−Boltzmann distributions.[31,46,47] We see that there is an inelastic collision with the surface, but the molecules are not thermally equilibrated with the surface, as the fitting temperature is greater than 20 K (Figure 5b).

We next examine the translational, vibrational, and rotational energy transfer upon impact with the CH_4 surface because trapping only occurs when a molecule loses enough energy to the surface (Figure 6). The incident projectiles contain no rotational energy (to be consistent with our supersonic beam expansion conditions)[3] so we calculated the rotational energy gain due to collisions with the surface; the vibrational and translational energy losses are calculated by taking the initial − final energy (in electronvolts) for each scattered trajectory. With increasing initial incident velocity, more energy (translational and vibrational) is lost to the surface while nevertheless still leading to the overall decrease in sticking probability

(Figure 3). For the translational energy at the faster incident velocity (Figure 6a), we see the largest divergence; CD_4 loses 2.07 eV to the surface compared to 1.67 eV for CH_4. *The larger translational energy loss for CD_4 is what enables it to be trapped on the surface with a greater relative probability.* Additionally, even at the highest velocity with 1100 K initial vibrational energy and 0 K initial rotational energy, both CH_4 and CD_4 lose less than 0.25 eV vibrational energy to the surface and gain less than 0.06 eV rotational energy (Figure 6b,c). We find that the vibrational energy lost and rotational energy gained are all at least an order of magnitude smaller than the translational energy lost to the surface. *This indicates that it is the translational energy exchange that dominates the condensation behavior between incident CH_4 and CD_4 and the CH_4 surface, leading to trapping of these molecules rather than rotational and vibrational energy exchange.*

As a comparison and to further generalize our energy exchange occurring for CH_4 and CD_4, we also ran additional trajectories for CH_3D, CH_2D_2, and CD_3H impinging on the 20 K CH_4 surface. These trajectories were for the highest initial velocity (4613 m/s), corresponding to kinetic energies of 1.93, 2.02, and 2.10 eV for CH_3D, CH_2D_2, and CD_3H, respectively. The trajectories contained vibrational energies sampled from a Boltzmann distribution at 1100 K and 0 K rotational energy to directly compare to CH_4 and CD_4. First, we examined the sticking probability (Figure 7) and found that the increased
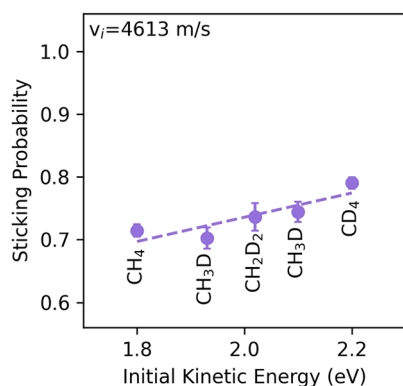
Figure 7. Sticking probabilities calculated from the number of 4613 m/s CH_4, CH_3D, CH_2D_2, and CD_3H, and CD_4 direct and physisorption trajectories scattering off a CH_4 surface at 20 K. Error bars represent the standard error of a binomial distribution of at least 1900 trajectories for CH_4 and CD_4 and between 400 and 800 trajectories for CH_3D, CH_2D_2, and CD_3H. The sticking probability increase is proportional to the number of deuterated atoms.

condensation is directly proportional to the number of deuterated atoms in the methane molecule. Thus, CD_4, with four deuterium atoms, has the highest sticking probability as compared to CH_4 and the other isotopologues (CH_3D, CH_2D_2, and CD_3H).

Next, we examine the translational energy loss (Figure 8a), vibrational energy loss (Figure 8b), and rotational gain (Figure 8c) for these five beams (CH_4, CH_3D, CH_2D_2, CD_3H, and CD_4) with the same initial velocity but increasing initial kinetic energies. We confirm that translational energy exchange dominates and is an order of magnitude higher than vibrational and rotational energy exchange. Additionally, the translational energy loss increases monotonically to preferentially trap the deuterated methane molecules.

Residence Time Distributions. To further understand how this translational energy loss is dissipated to trap the methane isotopologues, we examine their time on the surface (residence time). For all scattered trajectories, the residence time is the duration of time that an incident CH_4 or CD_4 has its center-of-mass (COM) height within 10 Å of the surface. The residence time distributions for the lowest velocity (2483 m/s) and highest velocity (4613 m/s) of CH_4/CD_4 molecules are shown in Figure 9a,b. These distributions are fit to an

exponentially modified Gaussian (EMG) function which is a convolution of an exponential and a Gaussian distribution probability distribution:[48]

$$h(t) = \frac{a}{\sqrt{\pi}} \exp\left[k(S - t) + \frac{(k\sigma)^2}{2}\right]\left[1 - \mathrm{erf}\left(\frac{S - t + k\sigma^2}{\sqrt{2}\,\sigma}\right)\right]$$

(2a)

where the complementary error function is defined as

$$\mathrm{erf}(z) = \frac{2}{\sqrt{\pi}} \int_0^z e^{-t^2}\, dt$$

(2b)

In eq 2a, a is the amplitude, σ is the Gaussian width, S is the skew or shift in the time from a normal Gaussian distribution, and k is the exponential decay. For the lowest velocity beams (Figure 9a), the CH_4 and CD_4 distributions are quite similar to Gaussian peak widths of ~0.3 ps, a relaxation time ($1/k$) of 0.77 ps, and an amplitude of 0.2. For the higher velocity beams, although both Gaussian widths are ~0.17 ps, there are some clear differences between the CH_4 and CD_4 results (Figure 9b). First, when considering the Gaussian component of the fit, CH_4 has a much higher amplitude (0.064) compared to CD_4 (0.048). Second, when considering the exponential decay component, the relaxation time is longer for CD_4 (1.31 ps) compared to CH_4 (0.98 ps). This supports the finding that CH_4 molecules spend less time interacting with the surface (1.5 vs 1.7 ps at the highest initial velocity).

Thus, we can clearly see in Figure 9c that with increasing initial velocity, on average, the molecules spend less time on the surface. To avoid convolution between different mechanisms, the average residence time on the surface (Figure 9c) considers only direct scattering trajectories. For these direct scattering trajectories, the translational energy loss during one bounce with the surface directly impacts the residence time. *We find that because CD_4 projectiles lose more translational energy to the surface during collision (particularly for the highest velocity beam), they end up interacting with the methane surface longer than the CH_4 projectiles and are therefore more likely to be trapped.*

Scattering Angle Distributions and 45° Incident Angle Trajectories. The final scattering angle (θ_f) is defined as the angle between the final velocity vector of CH_4 or CD_4 and the surface normal. With increasing incident velocity, the average scattered angle decreases for both CH_4 and CD_4, but it decreases more for CD_4. The final average angles are 48° and
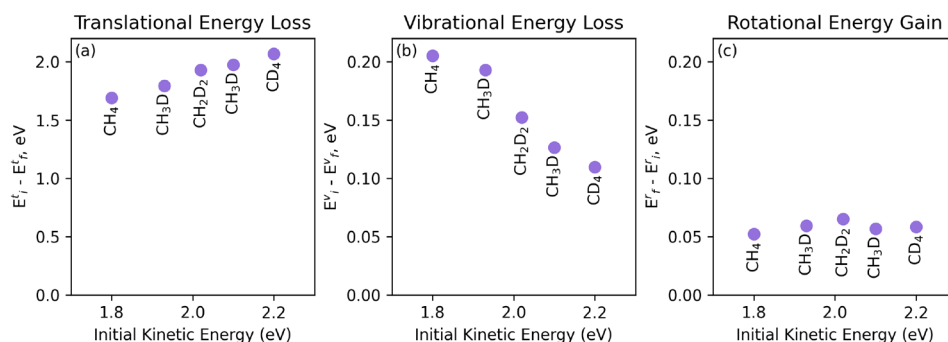
Figure 8. Average translational energy loss (a), vibrational energy loss (b), and rotational energy gain (c) for 4613 m/s CH_4, CH_3D, CH_2D_2, and CD_3H and CD_4 scattering off a CH_4 surface at 20 K. The methane and deuterated methane molecules have identical initial velocity (4613 m/s), vibrational energy (sampled from a Boltzmann at 1100 K), and 0 K rotational energy. The energy exchange is calculated using the momenta at the final step of the trajectory and the initial energy (in eV). Translational energy loss increases monotonically with increasing initial kinetic energy and is an order of magnitude higher than the vibrational and rotational energy.
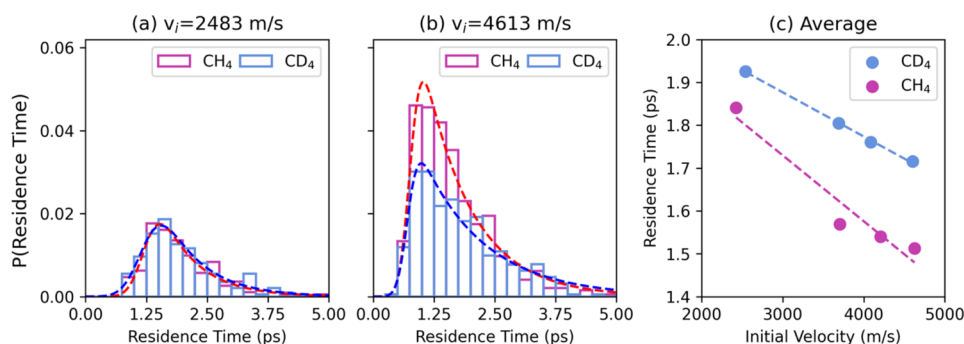
Figure 9. Residence time distribution of scattered CH_4 and CD_4 from a 20 K CH_4 surface. The residence time is the time in picoseconds during which the center-of-mass of CH_4 or CD_4 is within 10 Å of the surface. The distributions (panel a, v_i = 2483 m/s; panel b, v_i = 4613 m/s) are curve fit to an exponentially modified Gaussian (EMG). As the initial velocity increases, the average residence time (for the direct trajectories) on the surface (c) decreases; CH_4 spends less time on the surface compared to CD_4.

44° for CH_4 at the lowest and highest incident velocity, respectively, and 47° and 40° for CD_4. For all incident conditions, we find that the emitted trajectories do not scatter with a cosine distribution, indicating dominance of direct scattering and the lack of reemitted thermalized trajectories.

We also ran an additional set of simulations with trajectories that approach the surface from 45° instead of normal. The initial conditions for these trajectories were v_i = 2483 m/s and v_i = 4613 m/s with vibrational energy sampled from Boltzmann distributions at 300 and 1100 K, respectively, to match the experimental conditions and the trajectories impinging upon the surface at normal. We also included CH_4 and CD_4 trajectories with an initial velocity of 6579 m/s and vibrational energy sampled from a Boltzmann distribution at 1100 K so that the normal velocity component was 4613 m/s. In general, we find a lower overall sticking probability for trajectories incident at 45° versus normal. Therefore, our mechanism involving direct translational energy exchange with the intermolecular vibrations of the surface lattice upon one impact with the surface is broadly applicable regardless of the incident angle. Because the sticking probabilities are much lower for the 45° trajectories, we propose that perpendicular components of the incident momentum are especially important in this translational energy transfer to the surface lattice.

CONCLUSION

In conclusion, we performed detailed molecular dynamics simulations to understand our experimental result of differential condensation between CH_4 isotopologues impinging onto a CH_4 surface at 20 K. First, we have good agreement between our MD simulations and our experimental results, where there was increased adsorption of CD_4 compared to CH_4, particularly for the highest velocity beam. Second, we find that gas–surface collisional energy accommodation is dominated translational energy exchange with intermolecular vibrations of the methane surface lattice. CD_4 preferential sticking arises from its propensity to lose more energy during its first impact with the surface, inducing longer residence times and leading to increased probability of becoming trapped and condensed onto the surface. Systematic trends are seen for sticking probabilities and energy transfer when we explore the behavior of the other H/D substituted isotopologues of methane.

In general, our increased understanding of this gas–surface energy exchange under non-equilibrium conditions at cold substrate temperatures from these numerical simulations has important astrophysical and technological implications. Two such technological applications are water condensation in high-velocity gas flows as experienced by aircraft in low-temperature situations and condensation on windmill blades for power generation operating in cold environments.

Importantly, these results offer a novel route for isotope enrichment and separation via the preferential condensation of heavier isotopes during gas–surface collisions under carefully selected substrate, gas mixture, kinematic, and incident velocity conditions.

These novel trapping efficiency differences and energy exchange mechanisms can also be incorporated into astrophysical models. Adsorption is often the first step for many cold temperature reactions occurring on dust grains, with trapping efficiency differences having notable implications for allowed reaction probabilities and subsequent events, leading to increased molecular complexity. Our investigations of gas–surface collisional energy transfer processes can help to not only explain increased abundance of deuterium in solar system planets,[53,54] but these mechanisms can be incorporated into astrophysical models of the icy dust grain processes including those in the interstellar region.[5]

■ AUTHOR INFORMATION

Corresponding Author
S. J. Sibener − *The James Franck Institute and Department of Chemistry, The University of Chicago, Chicago, Illinois 60637, United States;* ⊙ orcid.org/0000-0002-5298-5484; Email: s-sibener@uchicago.edu

Authors
Michelle R. Brann − *The James Franck Institute and Department of Chemistry, The University of Chicago, Chicago, Illinois 60637, United States;* ⊙ orcid.org/0000-0002-9889-3921

Xinyou Ma − *The James Franck Institute and Department of Chemistry, The University of Chicago, Chicago, Illinois 60637, United States;* ⊙ orcid.org/0000-0002-0923-8758

Complete contact information is available at:
https://pubs.acs.org/10.1021/acs.jpcc.3c02386

Notes
The authors declare no competing financial interest.

■ REFERENCES

(1) Nogueira, J. J.; Hase, W. L.; Martínez-Núñez, E. Understanding Energy Transfer in Gas-Surface Collisions from Gas-Phase Models. *J. Phys. Chem. C* **2014**, *118*, 2609−2621.

(2) Rettner, C. T.; Auerbach, D. J.; Tully, J. C.; Kleyn, A. W. Chemical Dynamics at the Gas-Surface Interface. *J. Phys. Chem.* **1996**, *100*, 13021−13033.

(3) Brann, M. R.; Hansknecht, S. P.; Ma, X.; Sibener, S. J. Differential Condensation of Methane Isotopologues Leading to Isotopic Enrichment under Non-Equilibrium Gas-Surface Collision Conditions. *J. Phys. Chem. A* **2021**, *125*, 9405−9413.

(4) Burke, D. J.; Brown, W. A. Ice in Space: Surface Science Investigations of the Thermal Desorption of Model Interstellar Ices on Dust Grain Analogue Surfaces. *Phys. Chem. Chem. Phys.* **2010**, *12*, 5947−5969.

(5) Hama, T.; Watanabe, N. Surface Processes on Interstellar Amorphous Solid Water: Adsorption, Diffusion, Tunneling Reactions, and Nuclear-Spin Conversion. *Chem. Rev.* **2013**, *113*, 8783−8839.

(6) Watanabe, N.; Kouchi, A. Ice Surface Reactions: A Key to Chemical Evolution in Space. *Prog. Surf. Sci.* **2008**, *83*, 439−489.

(7) Licandro, J.; Pinilla-Alonso, N.; Pedani, M.; Oliva, E.; Tozzi, G. P.; Grundy, W. M. The Methane Ice Rich Surface of Large TNO 2005 FY9: A Pluto-Twin in the Trans-Neptunian Belt? *Astron. Astrophys.* **2006**, *445*, L35−38.

(8) Merlin, F.; Alvarez-Candal, A.; Delsanti, A.; Fornasier, S.; Barucci, M. A.; Demeo, F. E.; De Bergh, C.; Doressoundiram, A.; Quirico, E.; Schmitt, B. Stratification of Methane Ice on Eris' Surface. *Astron. J.* **2009**, *137*, 315−328.

(9) Brown, M. E.; Trujillo, C. A.; Rabinowitz, D. L. Discovery of a Planetary-Sized Object in the Scattered Kuiper Belt. *Astrophys. J.* **2005**, *635*, 97−100.

(10) Licandro, J.; Grundy, W. M.; Pinilla-Alonso, N.; Leisy, P. Visible Spectroscopy of 2003 UB313: Evidence for N_2 Ice on the Surface of the Largest TNO? *Astron. Astrophys.* **2006**, *458*, L5−8.

(11) Dumas, C.; Merlin, F.; Barucci, M. A.; De Bergh, C.; Hainault, O.; Guilbert, A.; Vernazza, P.; Doressoundiram, A. Surface Composition of the Largest Dwarf Planet 136199 Eris (2003UB 313). *Astron. Astrophys.* **2007**, *471*, 331−334.

(12) Tokano, T.; McKay, C. P.; Neubauer, F. M.; Atreya, S. K.; Ferri, F.; Fulchignoni, M.; Niemann, H. B. Methane Drizzle on Titan. *Nature* **2006**, *442*, 432−435.

(13) Merlin, F. New Constraints on the Surface of Pluto. *Astron. Astrophys.* **2015**, *582*, A39.

(14) Di Corcia, A.; Liberti, A. Isotope Effect on Physical Adsorption. *Trans. Faraday Soc.* **1970**, *66*, 967−975.

(15) Bossa, J. B.; Paardekooper, D. M.; Isokoski, K.; Linnartz, H. Methane Ice Photochemistry and Kinetic Study Using Laser Desorption Time-of-Flight Mass Spectrometry at 20 K. *Phys. Chem. Chem. Phys.* **2015**, *17*, 17346−17354.

(16) Wang, X.; Schultz, A. J.; Halpern, Y. Kinetics of Methane Hydrate Formation from Polycrystalline Deuterated Ice. *J. Phys. Chem. A* **2002**, *106*, 7304−7309.

(17) Lanzerotti, L. J.; Brown, W. L.; Marcantonio, K. J. Experimental Study of Erosion of Methane Ice by Energetic Ions and Some Considerations for Astrophysics. *Astrophys. J.* **1987**, *313*, 910−919.

(18) Jones, B. M.; Kaiser, R. I. Application of Reflectron Time-of-Flight Mass Spectroscopy in the Analysis of Astrophysically Relevant Ices Exposed to Ionization Radiation: Methane (CH_4) and D4-Methane (CD_4) as a Case Study. *J. Phys. Chem. Lett.* **2013**, *4*, 1965−1971.

(19) Boogert, A. C. A.; Gerakines, P. A.; Whittet, D. C. B. Observations of the Icy Universe. *Annu. Rev. Astron. Astrophys.* **2015**, *53*, 541−581.

(20) Niemann, H. B.; Atreya, S. K.; Bauer, S. J.; Carignan, G. R.; Demick, J. E.; Frost, R. L.; Gautier, D.; Haberman, J. A.; Harpold, D. N.; Hunten, D. M.; et al. The Abundances of Constituents of Titan's Atmosphere from the GCMS Instrument on the Huygens Probe. *Nature* **2005**, *438*, 779−784.

(21) Abplanalp, M. J.; Góbi, S.; Kaiser, R. I. On the Formation and the Isomer Specific Detection of Methylacetylene (CH_3CCH), Propene (CH_3CHCH_2), Cyclopropane ($c\text{-}C_3H_6$), Vinylacetylene (CH_2CHCCH), and 1,3-Butadiene ($CH_2CHCHCH_2$) from Interstellar Methane Ice Analogues. *Phys. Chem. Chem. Phys.* **2019**, *21*, 5378−5393.

(22) He, J.; Gao, K.; Vidali, G.; Bennett, C. J.; Kaiser, R. I. Formation of Molecular Hydrogen from Methane Ice. *Astrophys. J.* **2010**, *721*, 1656−1662.

(23) Hase, W. L.; Duchovic, R. J.; Hu, X.; Komornicki, A.; Lim, K. F.; Lu, D.-H.; Peslherbe, G. H.; Swamy, K. N.; Vande Linde, S. R.; Varandas, A.; et al. VENUS96: A General Chemical Dynamics Computer Program. *Quantum Chem. Prog. Exch. Bull.* **1996**, *16*, 43.

(24) Barnes, G. L.; Hase, W. L. Energy Transfer, Unfolding, and Fragmentation Dynamics in Collisions of N-Protonated Octaglycine with an H-SAM Surface. *J. Am. Chem. Soc.* **2009**, *131*, 17185−17193.

(25) Yan, T.; Hase, W. L. Origin of the Boltzmann Translational Energy Distribution in the Scattering of Hyperthermal Ne Atoms off a Self-Assembled Monolayer. *Phys. Chem. Chem. Phys.* **2000**, *2*, 901−910.

(26) Jiang, B.; Guo, H. Mode and Bond Selectivities in Methane Dissociative Chemisorption: Quasi-Classical Trajectory Studies on Twelve-Dimensional Potential Energy Surface. *J. Phys. Chem. C* **2013**, *117*, 16127−16135.

(27) Jiang, B.; Xie, D.; Guo, H. Vibrationally Mediated Bond Selective Dissociative Chemisorption of HOD on Cu(111). *Chem. Sci.* **2013**, *4*, 503−508.

(28) Hase, W. L.; Date, N.; Bhuiyan, L. B.; Buckowski, D. G. Energy Transfer in Collisions of Ar with Highly Excited Water and Methane. *J. Phys. Chem.* **1985**, *89*, 2502−2507.

(29) Gibson, K. D.; Killelea, D. R.; Yuan, H.; Becker, J. S.; Pratihar, S.; Manikandan, P.; Kohale, S. C.; Hase, W. L.; Sibener, S. J. Scattering of High-Incident-Energy Kr and Xe from Ice: Evidence That a Major Channel Involves Penetration into the Bulk. *J. Phys. Chem. C* **2012**, *116*, 14264−14273.

(30) Majumder, M.; Gibson, K. D.; Sibener, S. J.; Hase, W. L. Chemical Dynamics Simulations and Scattering Experiments for O_2 Collisions with Graphite. *J. Phys. Chem. C* **2018**, *122*, 16048−16059.

(31) Pratihar, S.; Kohale, S. C.; Yang, L.; Manikandan, P.; Gibson, K. D.; Killelea, D. R.; Yuan, H.; Sibener, S. J.; Hase, W. L. Chemical Dynamics Simulations of High Energy Xenon Atom Collisions with the {0001} Surface of Hexagonal Ice. *J. Phys. Chem. C* **2013**, *117*, 2183−2193.

(32) Gibson, K. D.; Killelea, D. R.; Yuan, H.; Becker, J. S.; Sibener, S. J. Determination of the Sticking Coefficient and Scattering Dynamics of Water on Ice Using Molecular Beam Techniques. *J. Chem. Phys.* **2011**, *134*, 034703.

(33) Duchovic, R. J.; Hase, W. L.; Schlegel, H. B. Analytic Function for the $H + CH_3 \rightleftarrows CH_4$ Potential Energy Surface. *J. Phys. Chem.* **1984**, *88*, 1339−1347.

(34) Maynard-Casely, H. E.; Bull, C. L.; Guthrie, M.; Loa, I.; McMahon, M. I.; Gregoryanz, E.; Nelmes, R. J.; Loveday, J. S. The Distorted Close-Packed Crystal Structure of Methane A. *J. Chem. Phys.* **2010**, *133*, 064504−10.

(35) Severin, E. S.; Tildesley, D. J. A Methane Molecule Adsorbed on a Graphite Surface. *Mol. Phys.* **1980**, *41*, 1401−1418.

(36) Phillips, J. M.; Hammerbacher, M. D. Methane Adsorbed on Graphite. I. Intermolecular Potentials and Lattice Sums. *Phys. Rev. B* **1984**, *29*, 5859−5864.

(37) Heinz, H.; Vaia, R. A.; Farmer, B. L.; Naik, R. R. Accurate Simulation of Surfaces and Interfaces of Face-Centered Cubic Metals Using 12−6 and 9−6 Lennard-Jones Potentials. *J. Phys. Chem. C* **2008**, *112*, 17281−17290.

(38) Darling, S. B.; Rosenbaum, A. W.; Wang, Y.; Sibener, S. J. Coexistence of the $(23 \times \sqrt{3})$ Au(111) Reconstruction and a Striped Phase Self-Assembled Monolayer. *Langmuir* **2002**, *18*, 7462−7468.

(39) Hellmann, R.; Bich, E.; Vogel, E. Ab Initio Intermolecular Potential Energy Surface and Second Pressure Virial Coefficients of Methane. *J. Chem. Phys.* **2008**, *128*, 214303.

(40) Hirschfelder, J. O.; Curtiss, C. F.; Bird, R. B. *Molecular Theory of Gases and Liquids*; Wiley: New York, 1956; Vol. *17*.

(41) Ma, X.; Paul, A. K.; Hase, W. L. Chemical Dynamics Simulations of Benzene Dimer Dissociation. *J. Phys. Chem. A* **2015**, *119*, 6631−6640.

(42) Hu, X.; Hase, W. L.; Pirraglia, T. Vectorization of the General Monte Carlo Classical Trajectory Program VENUS. *J. Comput. Chem.* **1991**, *12*, 1014−1024.

(43) Hariharan, S.; Majumder, M.; Edel, R.; Grabnic, T.; Sibener, S. J.; Hase, W. L. Exploratory Direct Dynamics Simulations of $^3O_2$ Reaction with Graphene at High Temperatures. *J. Phys. Chem. C* **2018**, *122*, 29368−29379.

(44) King, D. A.; Wells, M. G. Molecular Beam Investigation of Adsorption Kinetics on Bulk Metal Targets: Nitrogen on Tungsten. *Surf. Sci.* **1972**, *29*, 454−482.

(45) Furue, H.; LeBlanc, J. F.; Pacey, P. D.; Whalen, J. M. Analytical Potential Energy Surface for Methane in Terms of Interatomic Forces. *Chem. Phys.* **1991**, *154*, 425−435.

(46) Gibson, K. D.; Isa, N.; Sibener, S. J. Experiments and Simulations of Hyperthermal Xe Interacting with an Ordered 1-Decanethiol/Au (111) Monolayer: Penetration Followed by High-Energy, Directed Ejection. *J. Phys. Chem. A* **2006**, *110*, 1469−1477.

(47) Tesa-Serrate, M. A.; Smoll, E. J.; Minton, T. K.; McKendrick, K. G. Atomic and Molecular Collisions at Liquid Surfaces. *Annu. Rev. Phys. Chem.* **2016**, *67*, 515−540.

(48) Grushka, E. Characterization of Exponentially Modified Gaussian Peaks in Chromatography. *Anal. Chem.* **1972**, *44*, 1733−1738.

(49) Rettner, C. T.; Schweizer, E. K.; Mullins, C. B. Desorption and Trapping of Argon at a 2H-W(100) Surface and a Test of the Applicability of Detailed Balance to a Nonequilibrium System. *J. Chem. Phys.* **1989**, *90*, 3800.

(50) Killelea, D. R.; Utz, A. L. On the Origin of Mode- and Bond-Selectivity in Vibrationally Mediated Reactions on Surfaces. *Phys. Chem. Chem. Phys.* **2013**, *15*, 20545−20554.

(51) Mastromatteo, M.; Jackson, B. The Dissociative Chemisorption of Methane on Ni(100) and Ni(111): Classical and Quantum Studies Based on the Reaction Path Hamiltonian. *J. Chem. Phys.* **2013**, *139*, 194701.

(52) Jackson, B.; Nave, S. The Dissociative Chemisorption of Methane on Ni(111): The Effects of Molecular Vibration and Lattice Motion. *J. Chem. Phys.* **2013**, *138*, 174705.

(53) Owen, T.; Maillard, J. P.; De Bergh, C.; Lutz, B. L. Deuterium on Mars: The Abundance of HDO and the Value of D/H. *Science* **1988**, *240*, 1767−1770.

(54) McCubbin, F. M.; Barnes, J. J. Origin and Abundances of H_2O in the Terrestrial Planets, Moon, and Asteroids. *Earth Planet. Sci. Lett.* **2019**, *526*, 115771.